

# *Future changes in atmospheric rivers and their implications for winter flooding in Britain*

Article

Supplemental Material

Lavers, D. A., Allan, R. P. ORCID: <https://orcid.org/0000-0003-0264-9447>, Villarini, G., Lloyd-Hughes, B., Brayshaw, D. J. ORCID: <https://orcid.org/0000-0002-3927-4362> and Wade, A. J. ORCID: <https://orcid.org/0000-0002-5296-8350> (2013) Future changes in atmospheric rivers and their implications for winter flooding in Britain. *Environmental Research Letters*, 8 (3). 034010. ISSN 1748-9326 doi: 10.1088/1748-9326/8/3/034010 Available at <https://centaur.reading.ac.uk/33434/>

It is advisable to refer to the publisher's version if you intend to cite from the work. See [Guidance on citing](#).

Published version at: <http://dx.doi.org/10.1088/1748-9326/8/3/034010>

To link to this article DOI: <http://dx.doi.org/10.1088/1748-9326/8/3/034010>

Publisher: Institute of Physics

All outputs in CentAUR are protected by Intellectual Property Rights law, including copyright law. Copyright and IPR is retained by the creators or other copyright holders. Terms and conditions for use of this material are defined in the [End User Agreement](#).

[www.reading.ac.uk/centaur](http://www.reading.ac.uk/centaur)

## **CentAUR**

Central Archive at the University of Reading

Reading's research outputs online

## Supplementary material

Table 1: The five CMIP5 climate models used in the study, with their availability of the simulations considered. Note that AMIP was unavailable for GFDL-ESM2G. The IVT thresholds are also shown.

Modelling Centre (or Group)	Model Name	Resolution (levels × latitudes × longitudes)	AMIP (1980– 2005)	Historical (1980– 2005)	RCP 4.5 (2074– 2099)	RCP 8.5 (2074– 2099)	IVT Threshold (kg m <sup>-1</sup> s <sup>-1</sup> )
Beijing Climate Center, China Meteorological Administration	BCC- CSM1.1	26 × 64 × 128 (312 km × 312 km)	Y	Y	Y	Y	437.4
Canadian Centre for Climate Modelling and Analysis	CanESM2	35 × 64 × 128 (312 km × 312 km)	Y	Y	Y	Y	437.4
Centre National de Recherches Météorologiques / Centre Européen de Recherche et Formation Avancées en Calcul Scientifique	CNRM- CM5	31 × 128 × 256 (156 km × 156 km)	Y	Y	Y	Y	343.9
NOAA Geophysical Fluid Dynamics Laboratory	GFDL- ESM2G	24 × 90 × 144 (222 km × 277.5 km)	N	Y	Y	Y	364.5
Norwegian Climate Centre	NorESM1- M	26 × 96 × 144 (208 km × 277.5 km)	Y	Y	Y	Y	479.0

Supplementary Figure 1 caption: Histograms of the number of time steps in the detected ARs in the five reanalyses and five CMIP5 models. The maximum number of time steps and the

skewness value are given in the panels for each distribution. (Positive skewness indicates a distribution skewed to the right.)

Supplementary Figure 2 caption: The cumulative distribution functions of the IVT during the ARs in the Historical (grey lines), RCP4.5 (green lines) and RCP8.5 (red lines) for the (a) bcc-csm1-1 model, (b) CanESM2 model, (c) CNRM-CM5 model, (d) GFDL-ESM2G model, and (e) NorESM1-M model. Panel f shows the average number of ARs per winter with the corresponding 2.5<sup>th</sup>-97.5<sup>th</sup> sampling confidence intervals.

Supplementary Figure 3 caption: Scatterplot of the low-level winds ( $\text{ms}^{-1}$ ) versus the low-level specific humidity ( $\text{g kg}^{-1}$ ) in the Historical (black) and RCP4.5 (red) runs of the bcc-csm1-1 model. Histograms of the marginal distributions are also shown. The Pearson product moment correlation coefficient (left) and p-value (right) between the low-level winds and specific humidity is shown for the Historical and RCP4.5 scenarios.

Supplementary Figure 4 caption: Scatterplot of the low-level winds ( $\text{ms}^{-1}$ ) versus the low-level specific humidity ( $\text{g kg}^{-1}$ ) in the Historical (black) and RCP8.5 (red) runs of the bcc-csm1-1 model. Histograms of the marginal distributions are also shown. The Pearson product moment correlation coefficient (left) and p-value (right) between the low-level winds and specific humidity is shown for the Historical and RCP8.5 scenarios.

Supplementary Figure 5 caption: Scatterplot of the low-level winds ( $\text{ms}^{-1}$ ) versus the low-level specific humidity ( $\text{g kg}^{-1}$ ) in the Historical (black) and RCP4.5 (red) runs of the CanESM2 model. Histograms of the marginal distributions are also shown. The Pearson product moment correlation coefficient (left) and p-value (right) between the low-level winds and specific humidity is shown for the Historical and RCP4.5 scenarios.

Supplementary Figure 6 caption: Scatterplot of the low-level winds ( $\text{ms}^{-1}$ ) versus the low-level specific humidity ( $\text{g kg}^{-1}$ ) in the Historical (black) and RCP8.5 (red) runs of the CanESM2 model. Histograms of the marginal distributions are shown. The Pearson product moment correlation coefficient (left) and p-value (right) between the low-level winds and specific humidity is shown for the Historical and RCP8.5 scenarios.

Supplementary Figure 7 caption: Scatterplot of the low-level winds ( $\text{ms}^{-1}$ ) versus the low-level specific humidity ( $\text{g kg}^{-1}$ ) in the Historical (black) and RCP4.5 (red) runs of the CNRM-CM5 model. Histograms of the marginal distributions are also shown. The Pearson product moment correlation coefficient (left) and p-value (right) between the low-level winds and specific humidity is shown for the Historical and RCP4.5 scenarios.

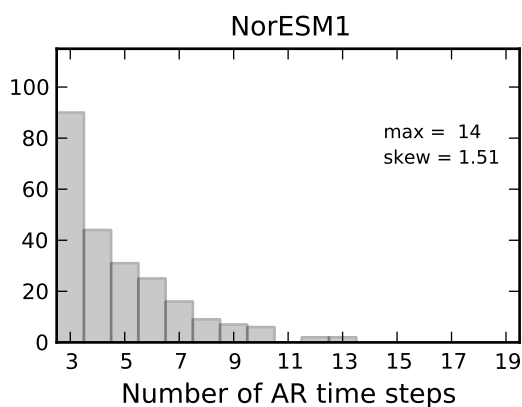
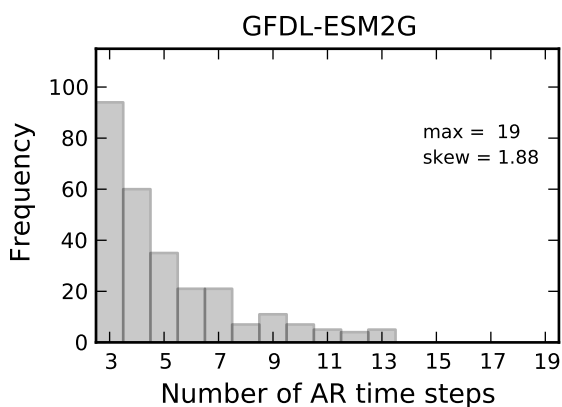
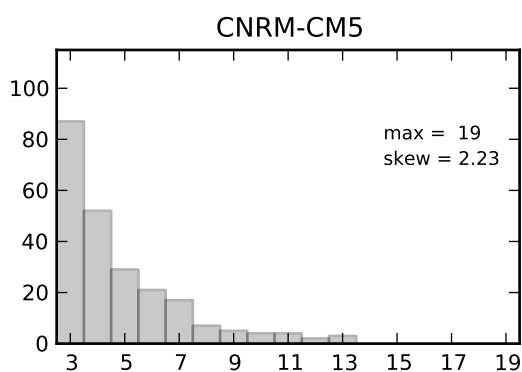
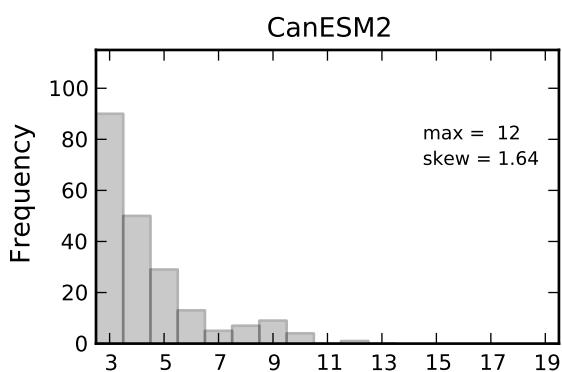
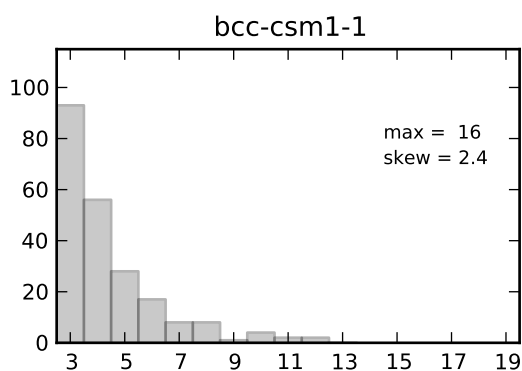
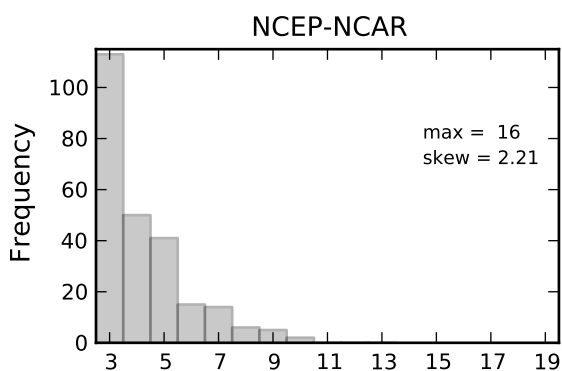
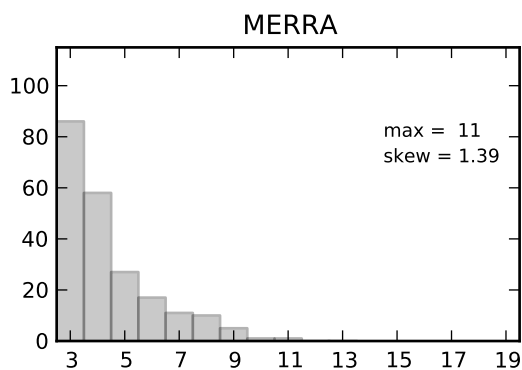
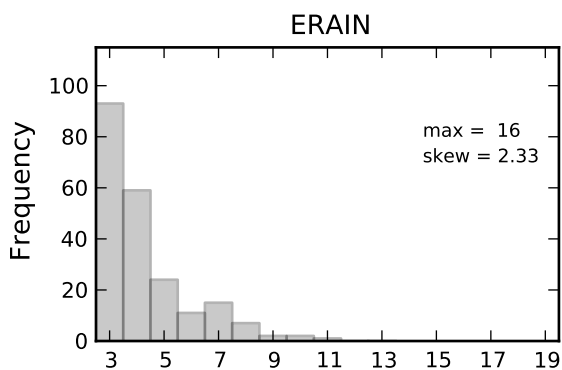
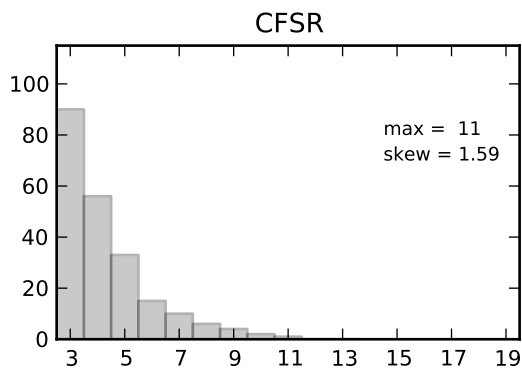
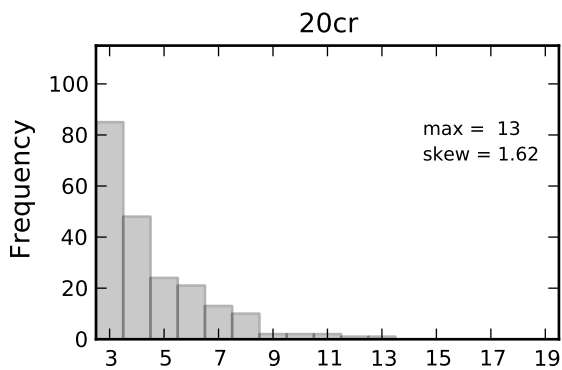
Supplementary Figure 8 caption: Scatterplot of the low-level winds ( $\text{ms}^{-1}$ ) versus the low-level specific humidity ( $\text{g kg}^{-1}$ ) in the Historical (black) and RCP8.5 (red) runs of the CNRM-CM5

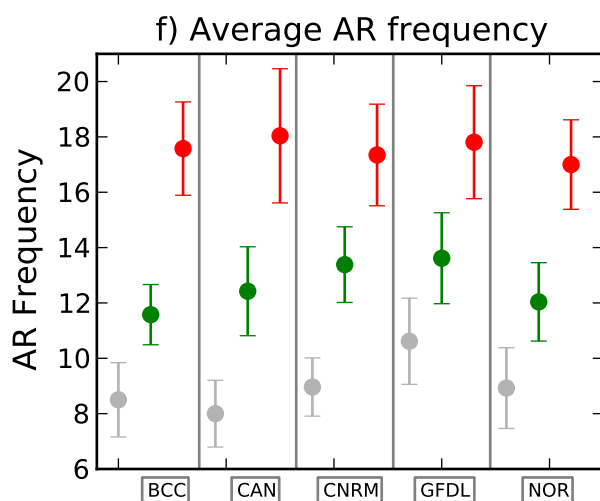
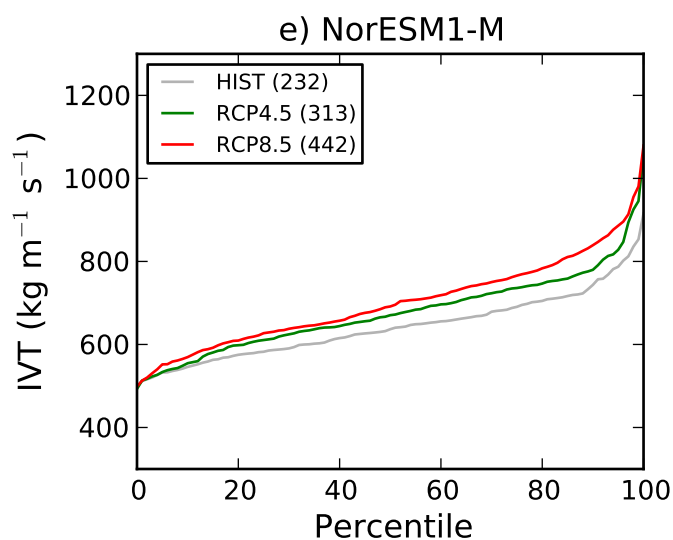
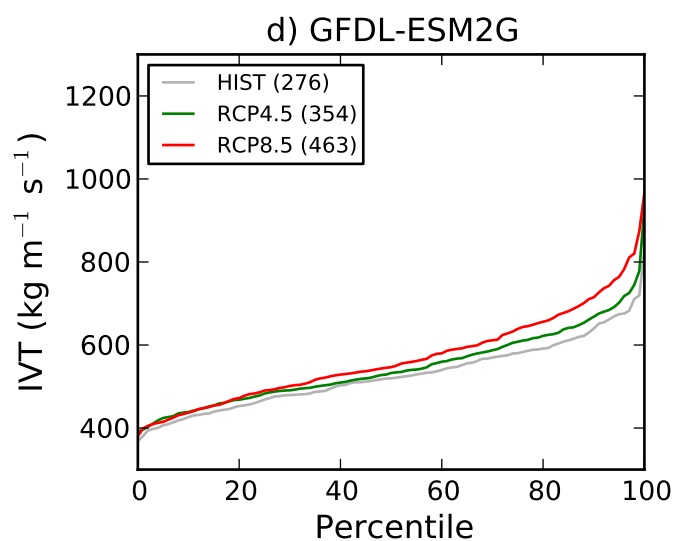
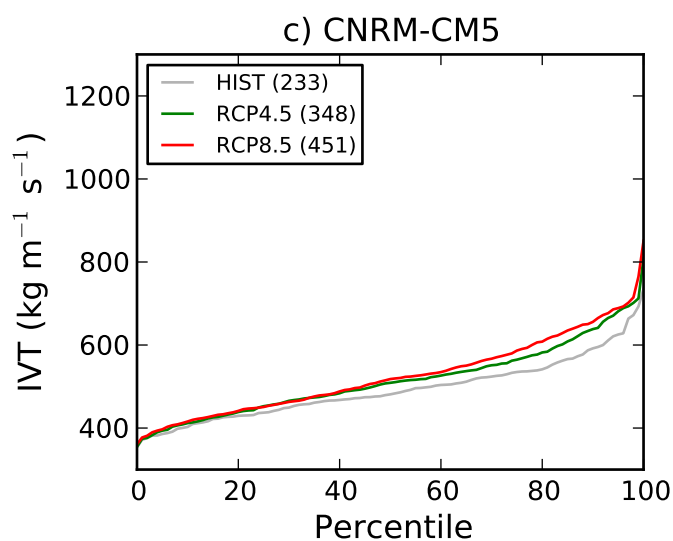
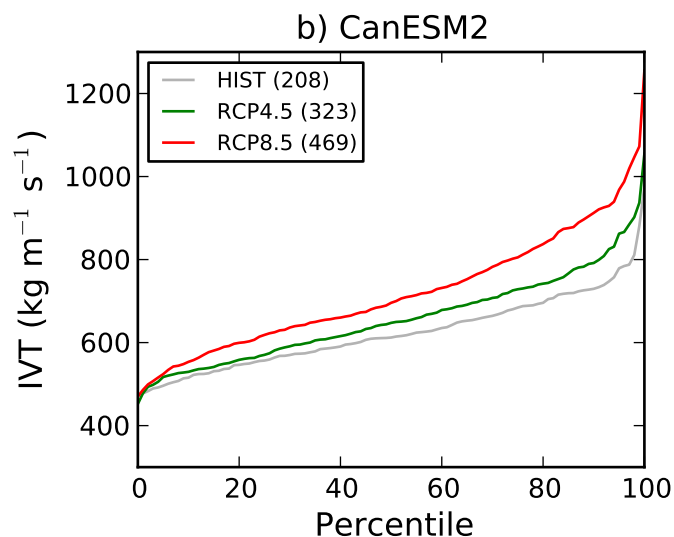
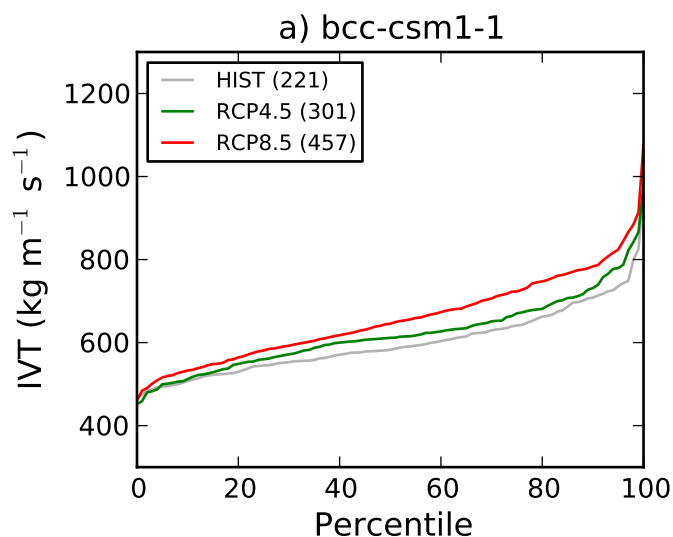
model. Histograms of the marginal distributions are shown. The Pearson product moment correlation coefficient (left) and p-value (right) between the low-level winds and specific humidity is shown for the Historical and RCP8.5 scenarios.

Supplementary Figure 9 caption: Scatterplot of the low-level winds ( $\text{ms}^{-1}$ ) versus the low-level specific humidity ( $\text{g kg}^{-1}$ ) in the Historical (black) and RCP4.5 (red) runs of the GFDL-ESM2G model. Histograms of the marginal distributions are also shown. The Pearson product moment correlation coefficient (left) and p-value (right) between the low-level winds and specific humidity is shown for the Historical and RCP4.5 scenarios.

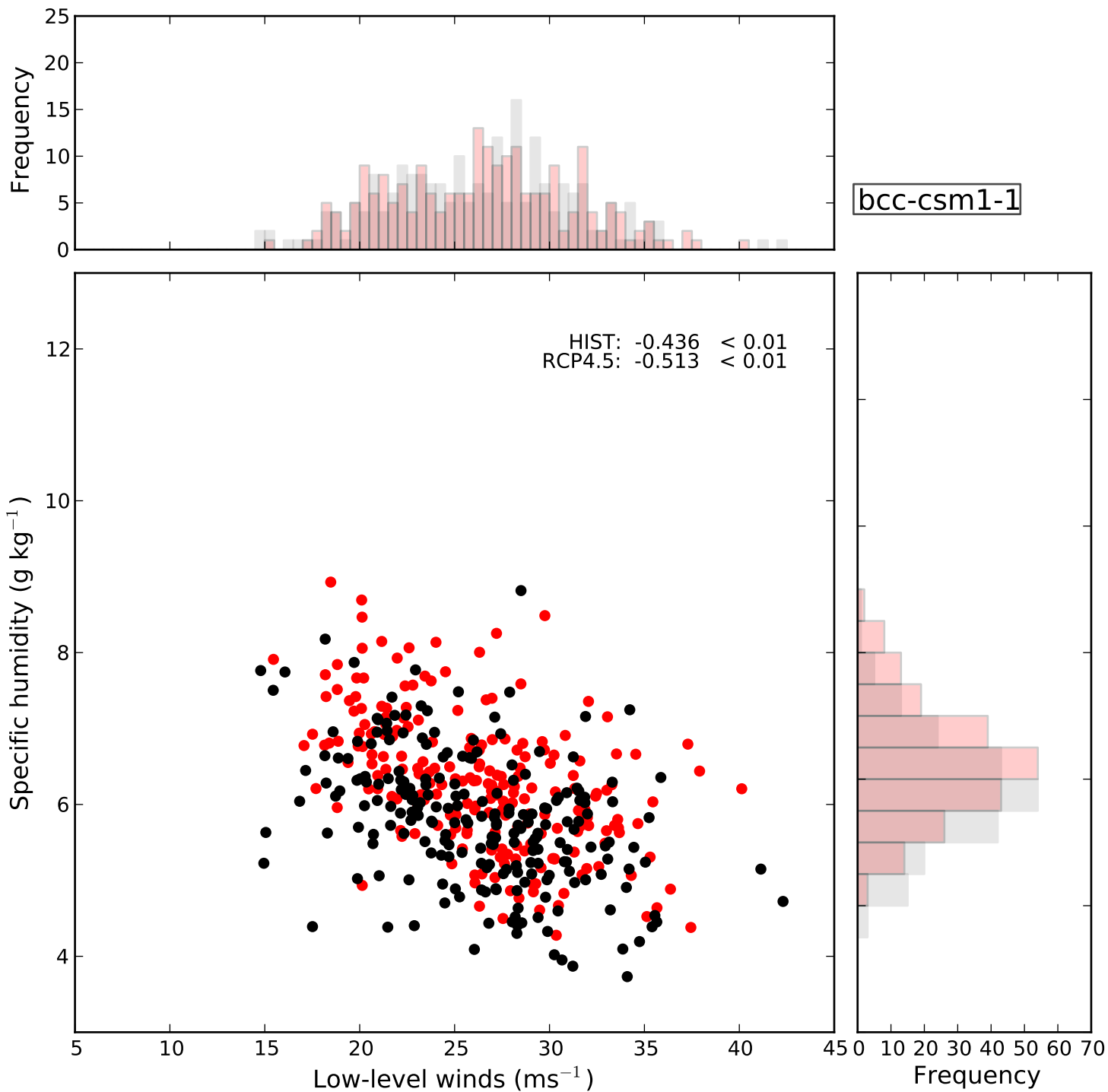
Supplementary Figure 10 caption: Scatterplot of the low-level winds ( $\text{ms}^{-1}$ ) versus the low-level specific humidity ( $\text{g kg}^{-1}$ ) in the Historical (black) and RCP8.5 (red) runs of the GFDL-ESM2G model. Histograms of the marginal distributions are shown. The Pearson product moment correlation coefficient (left) and p-value (right) between the low-level winds and specific humidity is shown for the Historical and RCP8.5 scenarios.

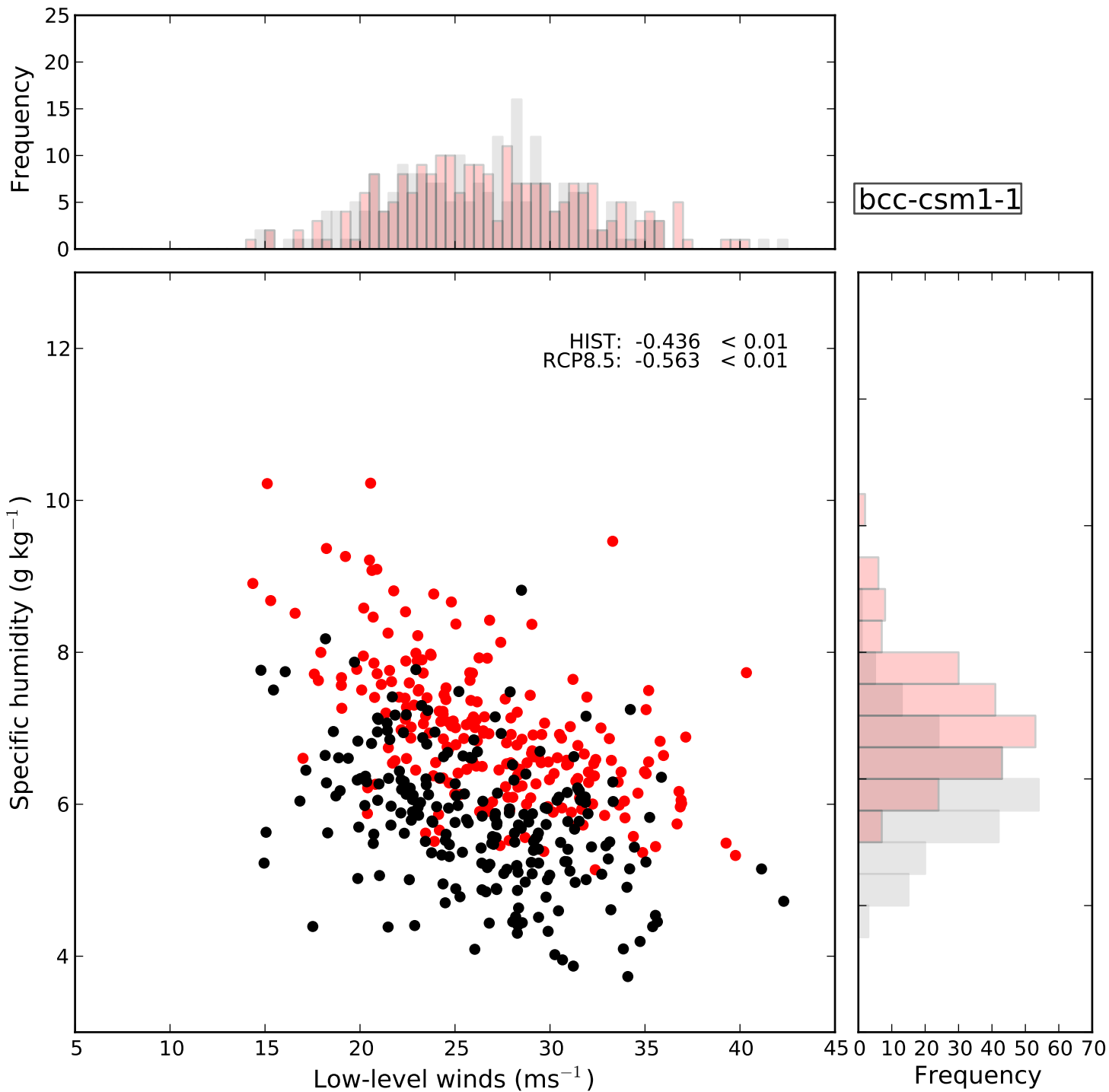
Supplementary Figure 11 caption: Scatterplot of the low-level winds ( $\text{ms}^{-1}$ ) versus the low-level specific humidity ( $\text{g kg}^{-1}$ ) in the Historical (black) and RCP4.5 (red) runs of the NorESM1-M model. Histograms of the marginal distributions are shown. The Pearson product moment correlation coefficient (left) and p-value (right) between the low-level winds and specific humidity is shown for the Historical and RCP4.5 scenarios.

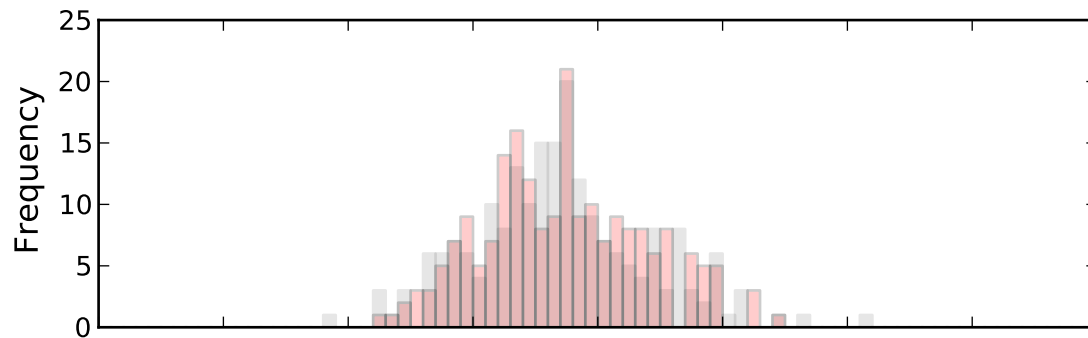




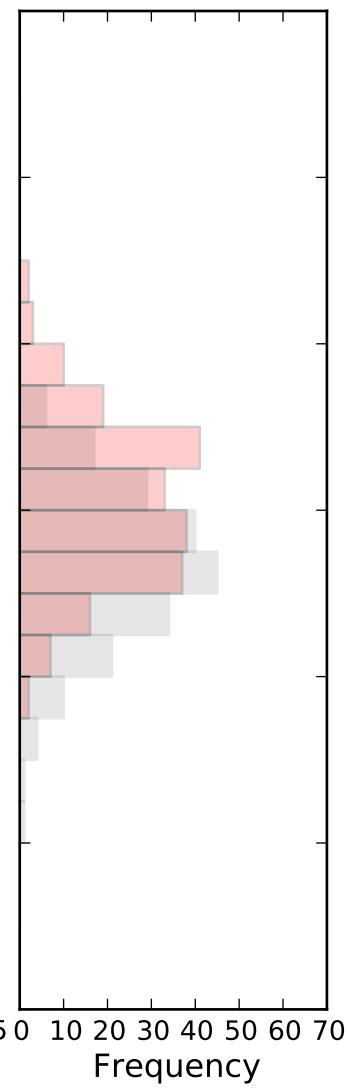
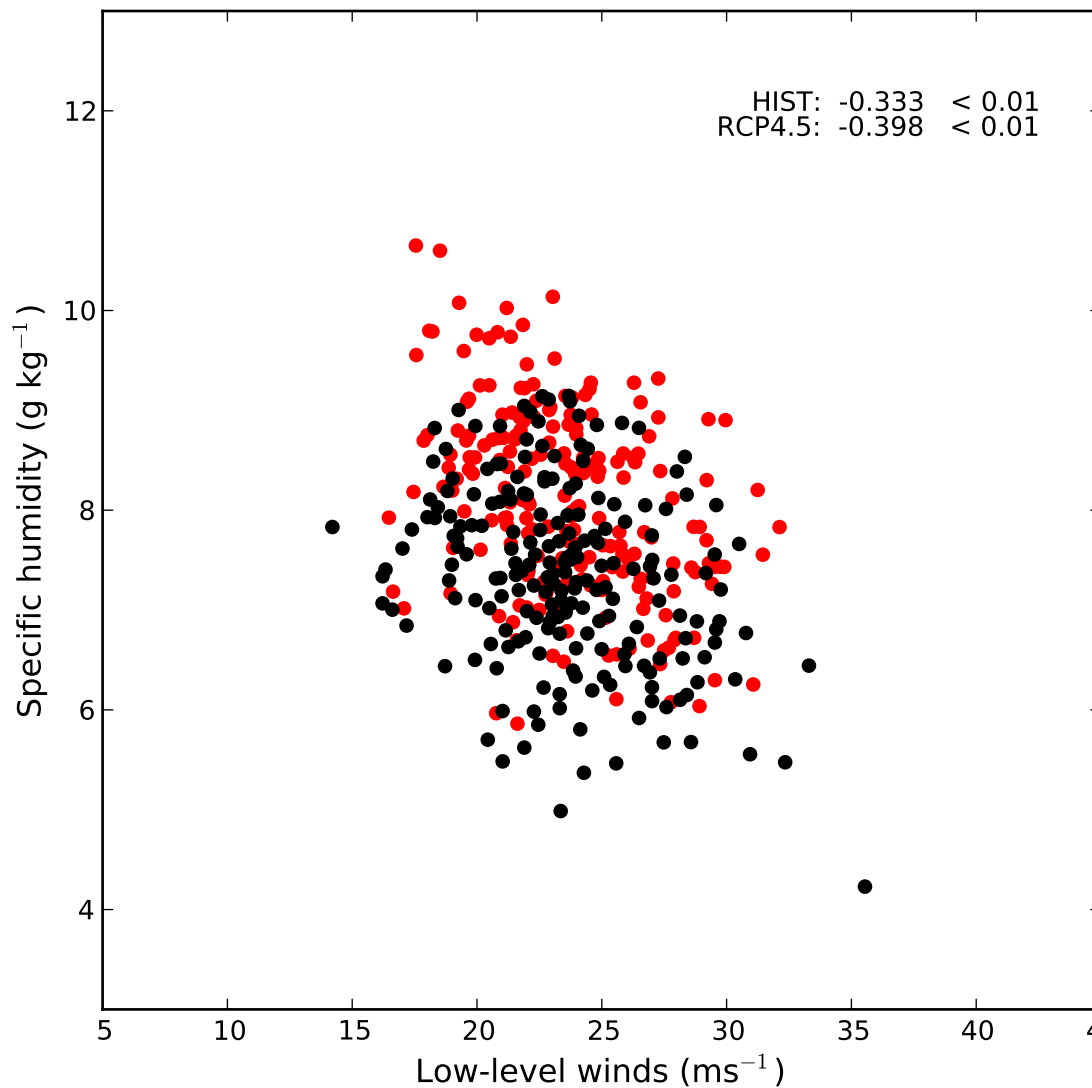


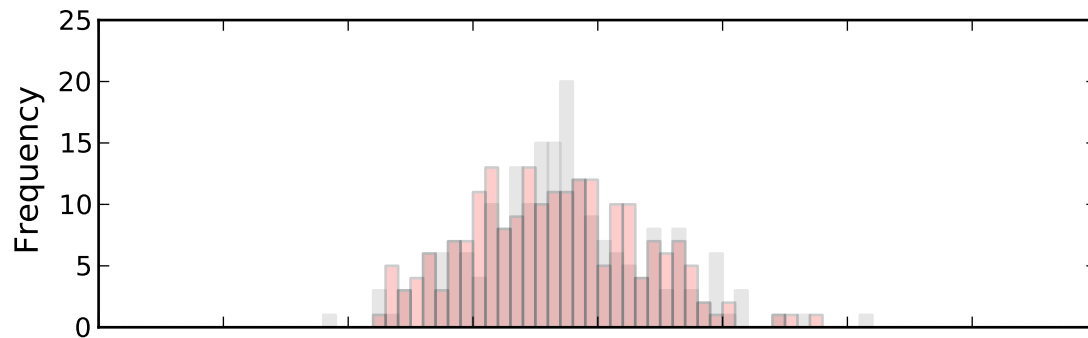




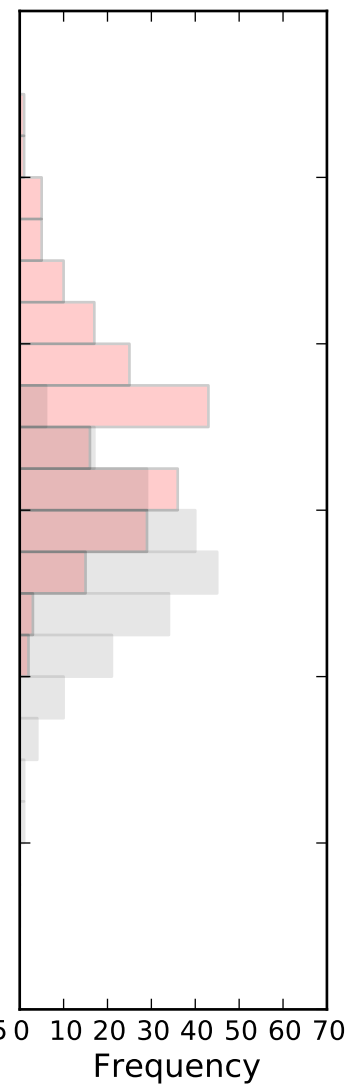
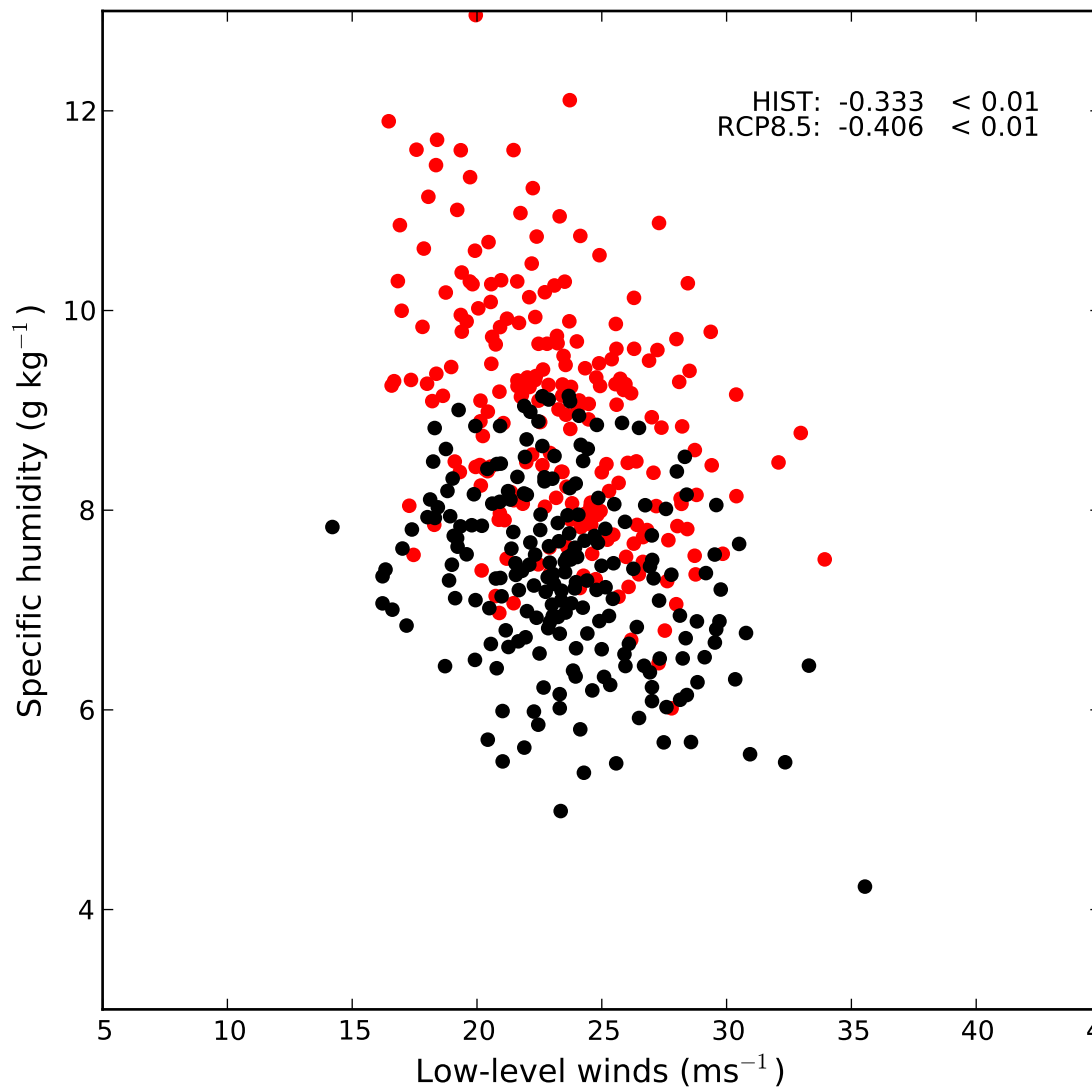


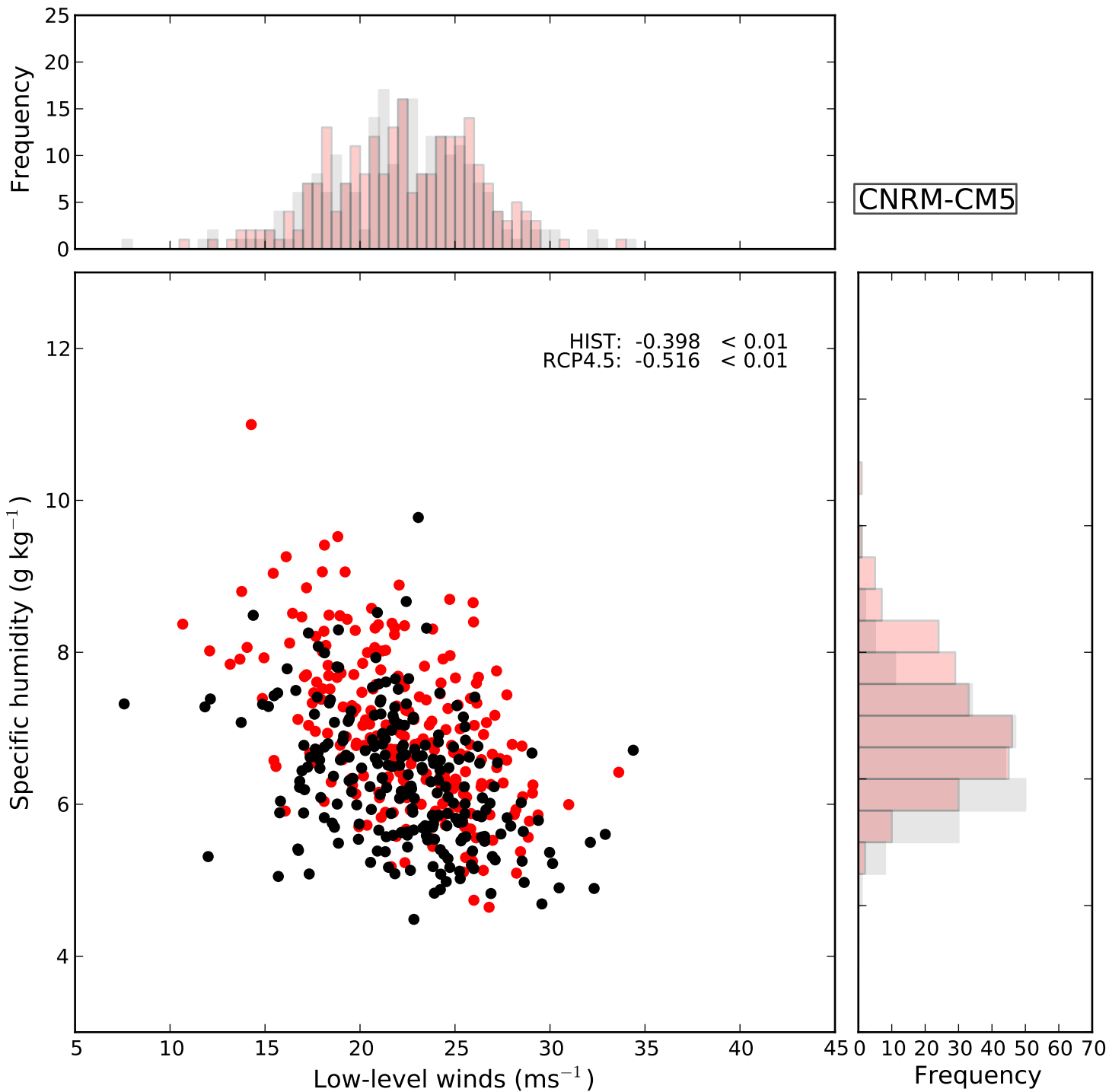
CanESM2

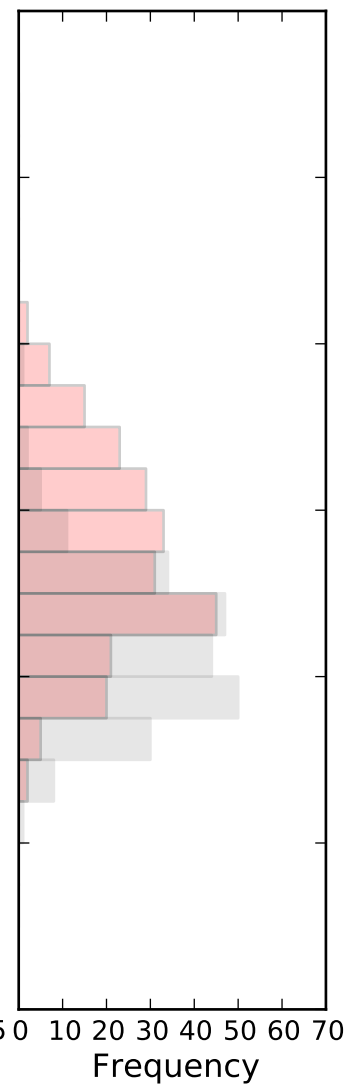
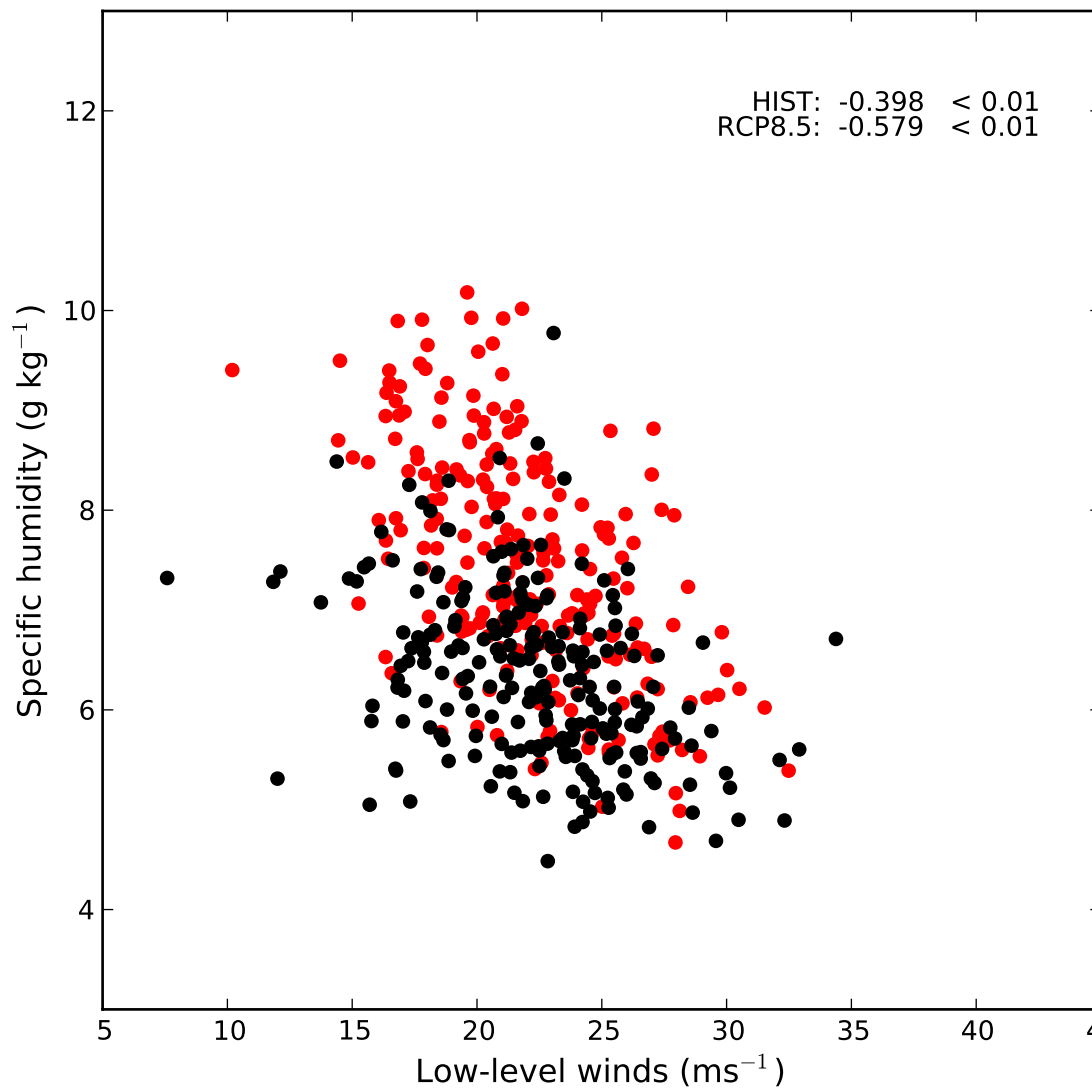
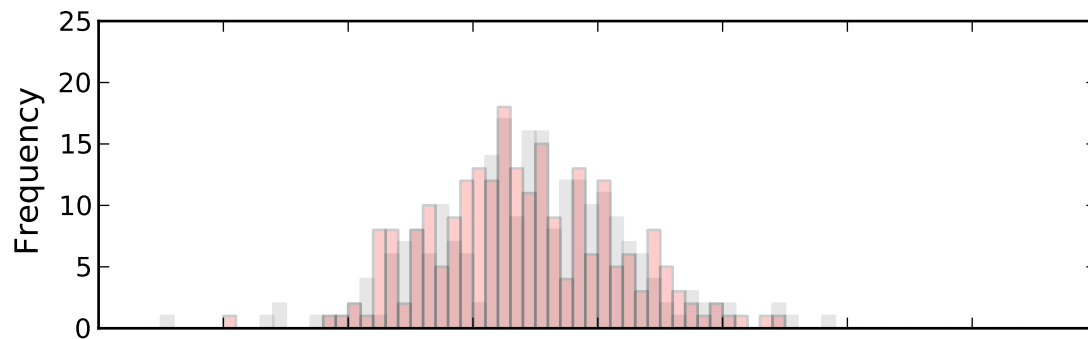


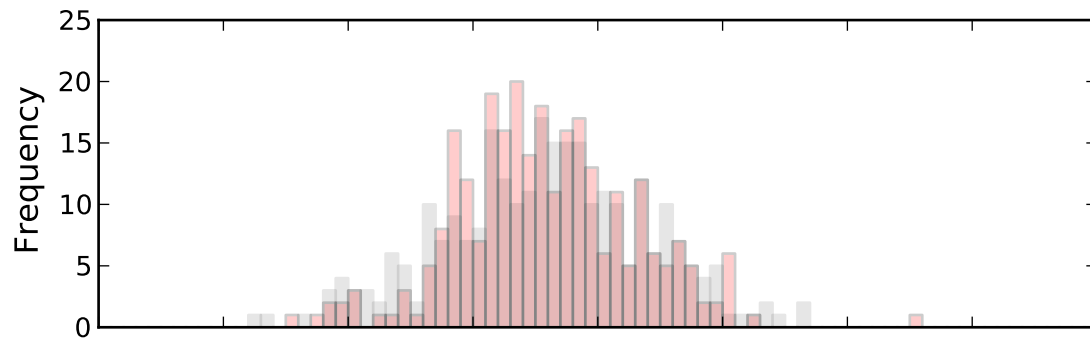


CanESM2

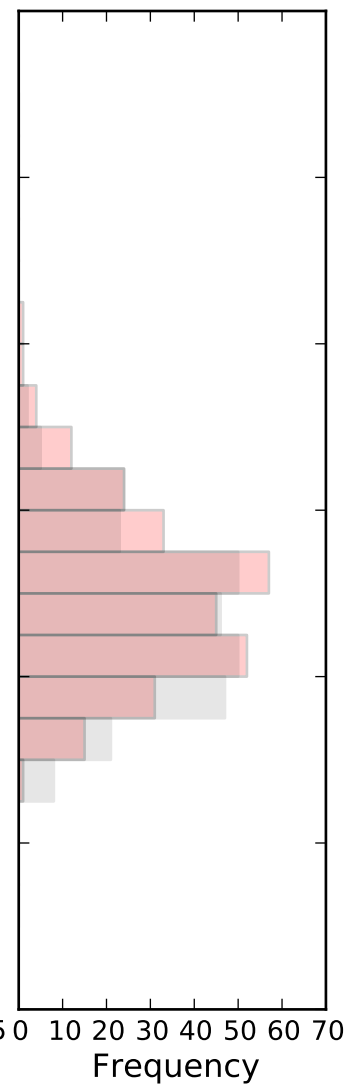
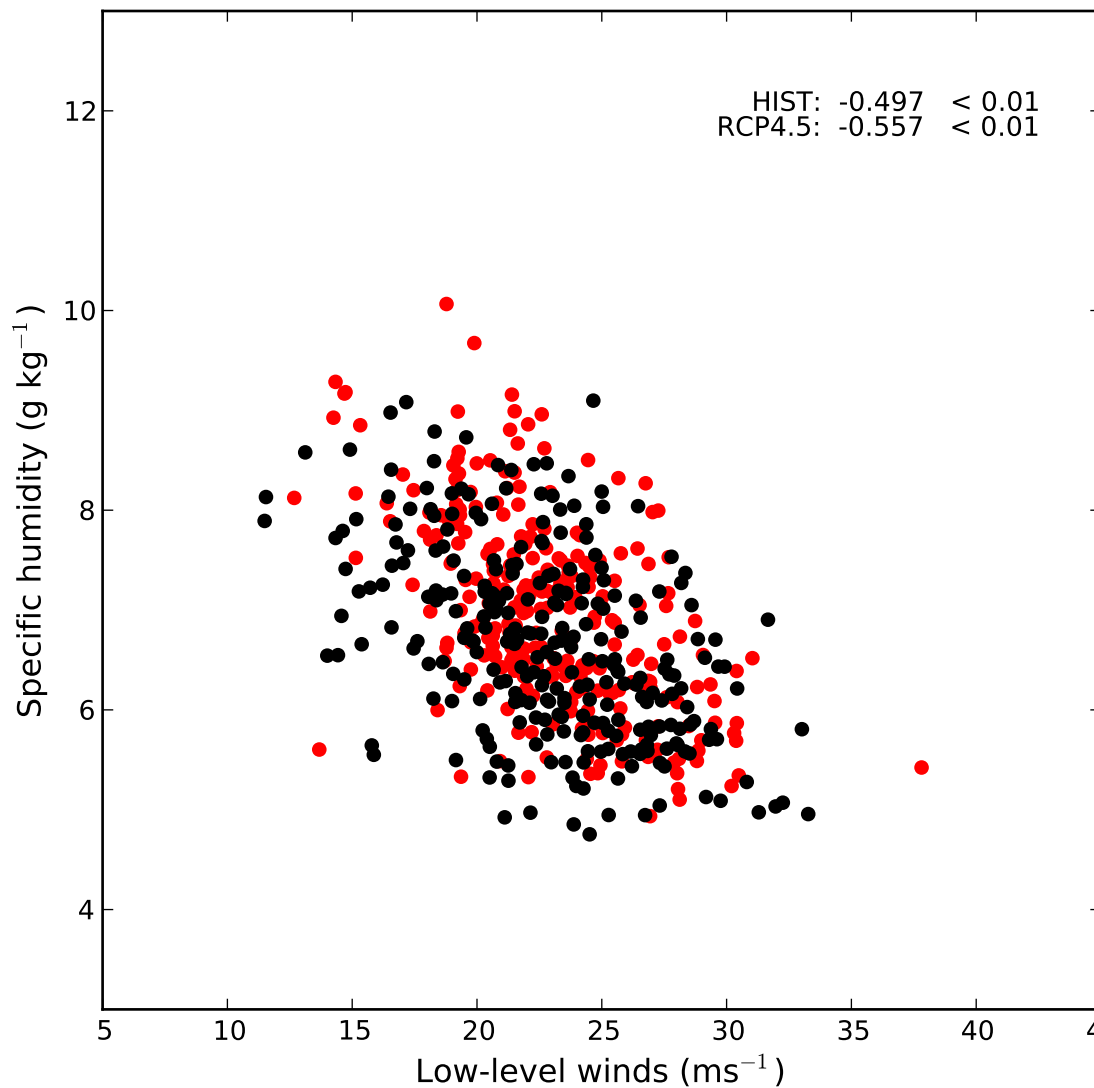


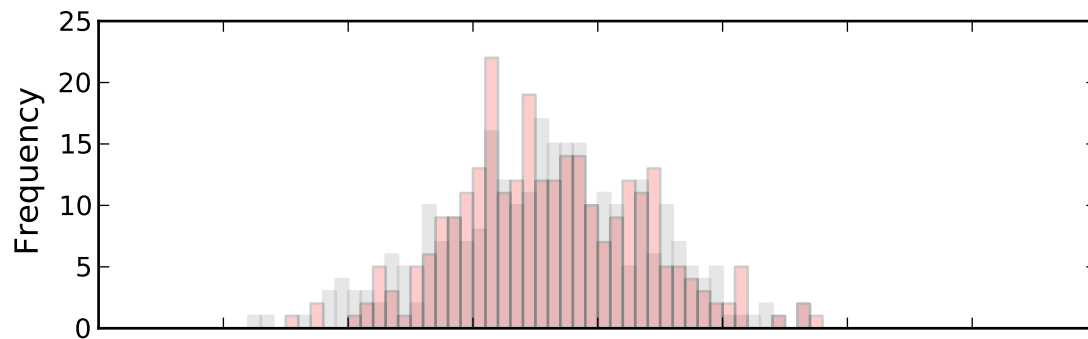




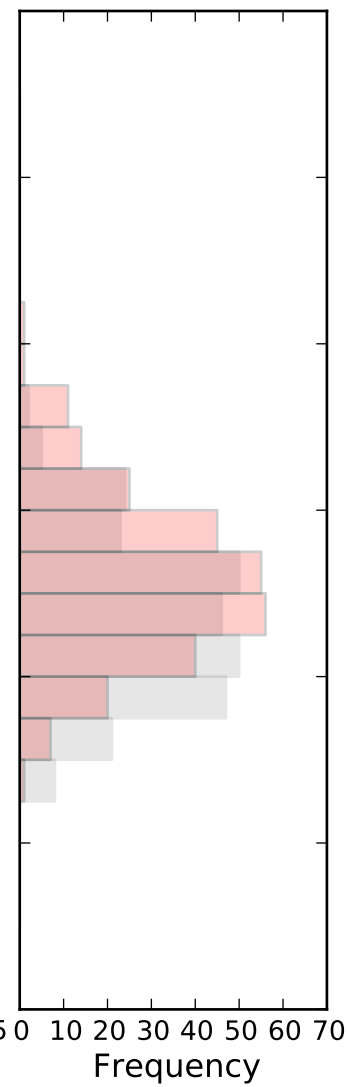
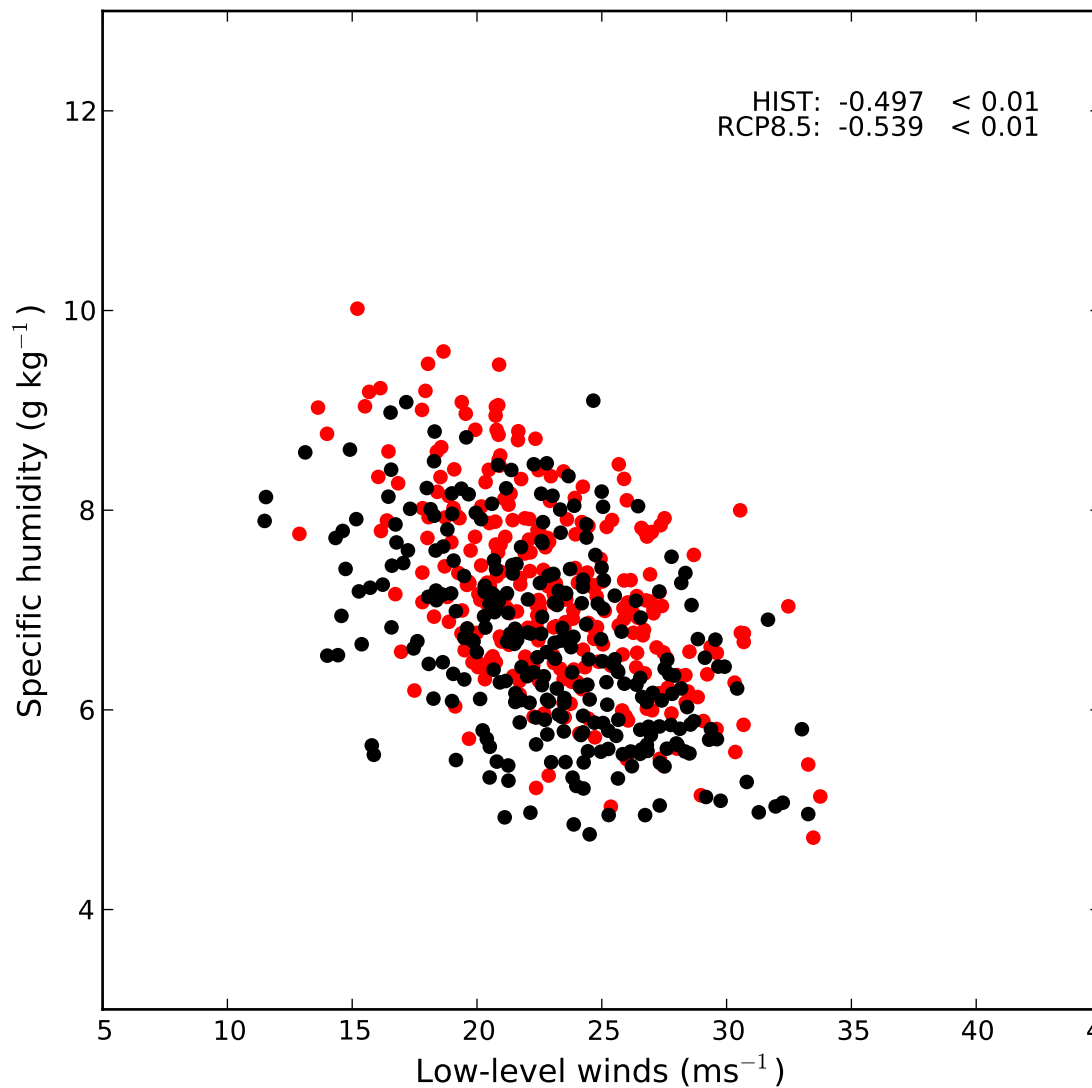


GFDL-ESM2G

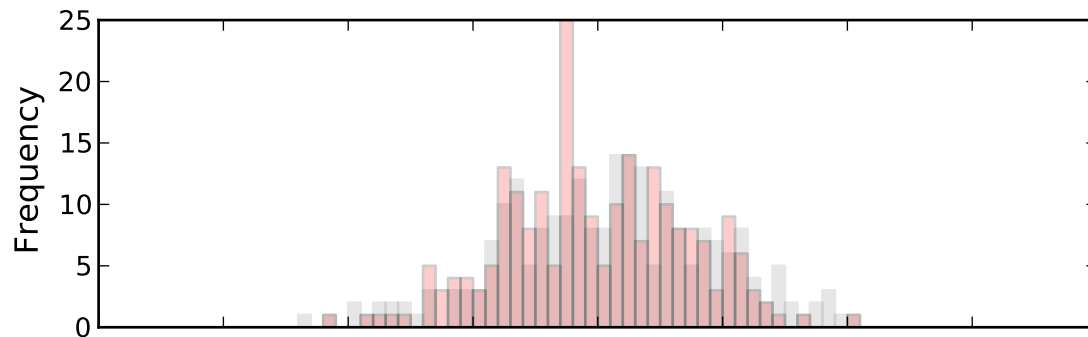




GFDL-ESM2G







NorESM1

